Parametric study of size, curvature and free edge effects on the predicted strength of bonded composite joints

Liu, Y, Lemanski, S & Zhang, X

DOI 10.1016/j.compstruct.2018.02.017
ISSN 0263-8223
ESSN 1879-1085
Publisher: Elsevier

Parametric study of size, curvature and free edge effects on the predicted strength of bonded composite joints

Yiding Liu, Stuart Lemanski, Xiang Zhang*

Centre for Manufacturing and Materials Engineering, Coventry University
Coventry, CV1 5FB, UK

* Corresponding author;

Email addresses: liuy116@uni.coventry.ac.uk; stuart.lemanski@coventry.ac.uk; xiang.zhang@coventry.ac.uk

Abstract

This paper presents the effects of size, curvature and free edges of laboratory lap joints on the debond fracture behaviour of joints that more realistically represent fuselage skin structures than conventional flat, narrow specimens. Finite Element Analysis is used in conjunction with Cohesive Zone Modelling (CZM) to predict the strength of selected joint features. The modelling approach was verified by simple single lap joint geometry. Four realistic joint features were then modelled by this validated modelling approach. The results show that moderate curvature has negligible effect on the peak load. There is a significant difference in the load vs displacement response of flat lab coupon joints with free edges and realistic curved joints with constrained edges. Further detail design features were investigated in this study, including (i) the joint runout and (ii) the presence of initial damage (thumbnail delamination). The modelling results show that the joggle configuration has an effect on the distribution of interlaminar stresses that affect the damage initiation and propagation. Fracture behaviour from different initial crack geometries associated with wider specimens has been simulated. From a design standpoint, an expansion of modelling capability is suggested to reduce the number of component tests in the traditional test pyramid.

Keywords: Aircraft composites; bonded joints; debond fracture; design study; finite element analysis

1. Introduction

There has been an increased use of composite materials in aircraft primary structures, especially of Carbon Fibre Reinforced Plastics (CFRPs) which are chosen for their high specific strength and stiffness. Composite structural components may be joined by adhesive bonding, or by mechanical fastening, or by a combination of adhesive and mechanical fastening. Adhesively bonded joints exhibit distinct advantages, such as ease of application, time and cost savings, and weight reduction [1, 2]. However, uncertainties regarding the quality of bonding, the presence of accidental damage, and the accurate prediction of the strength and damage tolerance performance of bonded composite joints currently require large safety factors to be applied at the design stage supplemented by an extensive testing programme [3].

Aircraft primary structural assemblies experience significant static and fatigue loadings in service. Analysis and testing is essential at the design stage to determine the structural integrity, durability and damage tolerance of the primary structures. However, full scale tests of large components are expensive and time consuming, which makes it impractical and inefficient to include every failure

scenario for the damage tolerant design philosophy. Research has so far focused on analytical, numerical and experimental investigations on idealised structural elements, e.g. the single lap joints (SLJ) [4-10]. The strength prediction of SLJ began with analytical methods by Volkersen [4] with simplified assumptions on material behaviour and boundary conditions. However, the mixed-mode damage behaviour makes the application of analytical methods difficult [5], which drove demand for accurate numerical simulations by FE analysis. Sawa and Liu [6] examined the stress distribution along the length of the adhesive in a SLJ using a 2D linear elastic finite element model. Goncalves et al. [7] developed a three-dimensional nonlinear FE analysis of adhesively bonded joints, which includes the stresses acting in the width direction and the effect of the bending moment. CZM have been used to predict the strength of SLJ with the thin layer of adhesive modelled as cohesive elements to simulate the interfacial fracture behaviour [8, 9]. Fully understanding the influence of CZM laws and parameters upon the predicted strength is of great importance. Campilho et al. [10] investigated the cohesive degradation (i.e. linear/bi-linear) of the adhesive on the accuracy of strength prediction of SLJs. Rocha et al. [11] evaluated different simulation conditions in the CZM analysis regarding elastic stiffness, mesh refinements and various damage initiation and growth criteria for the strength prediction of SLJs. However, research in [3-10] considered only flat lap joints. Limited information is available in the open literature on the mechanical performance of curved lap joints subjected to a complex combined loading condition to support the design of composite fuselage structures.

Longitudinal joints on fuselage skins are currently designed based on the results of static and fatigue load tests on simple uniaxially-loaded flat lap joint specimens. The use of uniaxial flat lap joint experimental data to design realistic lap joints for fuselage skins leads to uncertainties and sub-optimal design solutions, since the lab coupon joints are narrow, flat and have two free edges, whereas in realistic aircraft structures, lap joints are much wider, curved in shape, and connected to another structural part (i.e. with constrained edges). Therefore, several questions arise regarding the effects of these differences.

Regarding the influence of joint curvature on the strength and fracture behaviour, Ascione et al. [12] developed an extensive numerical investigation to predict the behaviour of curved adhesive joints subjected to axial loading, which accounts for the effect of curvature radius and the coupling between axial and shear behaviour corresponding to the cohesive laws. Their research highlighted that the influence of various curvature radius is insignificant in terms of mixed mode strain energy release rate (SERR) at the joint overlap. However, Parida et al. [13] employed 3D FEA simulation to study the effects of curvature of the curved composite panels on interlaminar stresses and three modes of SERR. The research found that flat SLJ have higher resistance to the delamination damage growth than curved SLJ. In reference [14], fatigue life for the curved specimens was observed to be significantly shorter than the flat specimens of the same dimensions.

Regarding the width and edge constraint, Muller [14] has evaluated the fatigue behaviour of flat riveted lap coupons in a metallic fuselage with various configurations in size and shape, and found that the total fatigue life for wide specimens with clamping pieces at the long edges in the longitudinal direction is always greater than for narrow specimens. Skorupa et al. [15] identified that the stress

distribution in metallic fuselage riveted lap joints is complex and non-uniform. A combination of hoop and longitudinal tension and out-of-plane bending of the skin is found under the effect of pressurization. The fatigue tests performed by Vlieger and Ottens [16] have found that the fatigue life under uniaxial loading can provide conservative results on the fatigue performance of biaxially loaded riveted specimens.

Considering the detailed design, the joggle feature can provide a perfectly smooth external elliptic shape to the cylindrical fuselage, e.g. to satisfy the aerodynamic requirement for a smooth external surface. Taib et al. [17] found that the localised curvature inherent to the joggle configuration plays a very important role in the stress distribution. However, the fracture response was not investigated.

For damage tolerant design requirement, realistic initial damage scenarios must be considered in the analysis and design. For the standard lab SLJ, i.e. flat and narrow width, initial damage is set at the joint runout ends and has a uniform size across its width. Due to the high interlaminar shear stresses at the bond overlap ends in the adhesive and very low tensile strength in the transverse direction (through-thickness), debond damage is likely occur. Ribeiro et al. [18] addressed the stress distributions in composite SLJs with different defect types and found that defects at the edges of the adhesive layer behabve more harmful to the joint's strength than the centred defects as the overlap ends transfer the main load. In a different work [19], the strength and damage growth in composite SLJs with various through-width and centered defective area and adhesive type have been studied using CZM predictive technique. Panigrahi et al. [5] calculated the SERRs variation along the damage front in a composite SLJ with a thorugh-width defect in adhesive failure and predicted an unstable delamination damage propagation along the overlap length. However, these researches [5, 18-19] only consider joints with standard geometry, i.e. flat, narrow width, and free long edges. Nevertheless, for a wide configuration, localised damage could be induced by accidental impact or lack of bonding, which may propagate under the fatigue loads. In general, the transferability of the laboratory test results from flat and narrow specimens to realistic structural joints still poses challenges.

So far, no studies have been found investigating the differences between the flat lap joint specimens and curved wide lap joints with features of the longitudinal joints in composite fuselage cover panels. Joints and joint features studied in this work are representative of the longitudinal joints in a commercial aircraft fuselage cover, which consists of several curved panels that are joined by adhesive bonding in the form of lap joints. In this parametric study, static strength and interlaminar fracture behaviour are studied by numerical modelling using an FE model that is validated by the single lap joint (SLJ) geometry. Three configurations were modelled: (a) curved lap joints, (b) lap joints with constrained long edges, (c) wider joints with different initial damage scenarios.

By performing this study, we contribute to the concept of Prediction Virtual Testing (PVT) proposed in reference [3]. The concept is described in Fig. 1, aiming to build a modified pyramid (Fig. 1b) which contains both flat and curved structural element features (Fig. 1c) to enhance the middle part of the traditional test pyramid and also to reduce the number of physical tests while improving the compliance demonstration for the proposed PVT test pyramid [3]. The modelling in the modified

pyramid is therefore used where possible so that the number of full scale tests of large components can be reduced with the support of small scale (i.e. lab coupons) and sub-component tests and using validated models to predict the behaviour of the full scale structures.

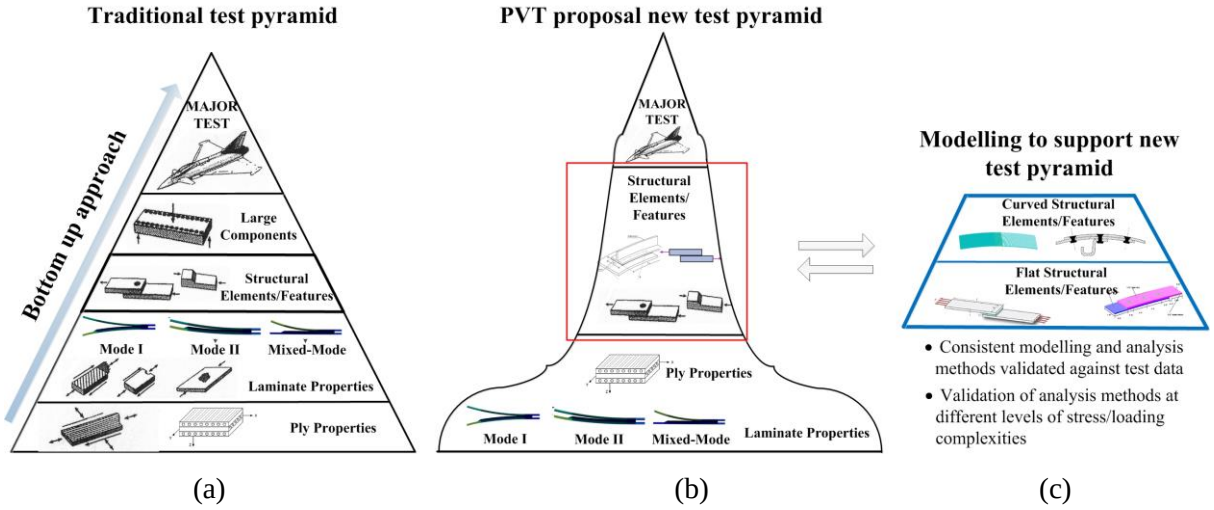

Fig. 1. (a) Example of current test pyramid, adopted from [20], (b) proposed test/analysis pyramid to support the predictive virtual testing (PVT) strategy [3], (c) features and models proposed in this paper that can replace/reduce physical tests in (b)

2. Modelling strategy and framework

This work studies the effect of different design features on the joint strength and fracture behaviour. These features include curvature, boundary conditions, detail design for bond run-out region and initial damage scenarios. Figure 2 summarises the ideas and focus of this study. The centre picture in Fig. 2 shows a curved lap joint with a number of realistic design features found in aircraft fuselage panel joints. The surrounding pictures (a) to (d) show typical design features that have been studied within this work. These are: (a) curved panels and joint, (b) constrained long edges owing to joint being part of a much wider structural panel, (c) joggled joint run-out to ensure aerodynamic shape and improve the bond strength, and (d) initial damage scenarios (e.g. due to accidental damage or bonding quality) to satisfy the damage tolerant design requirement. Considering the variation of these factors, different local models have been defined and grouped in four categories with model codes summarised in Table 1. All the analyses were performed by FEA using Abaqus code with geometrical nonlinearity.

Firstly, the well-known single lap joint (SLJ) geometry is used as a benchmark to validate the FE models in this study based on references [17, 21]. These validated models are subsequently used as the basis for the following design studies which investigated how the load vs. displacement response and stress distribution changed when realistic design features were included:

(a) Effect of curvature: Curved lap joint models were analysed with three different curvature radii (Fig. 2a). The strength is calculated by the cohesive zone modelling (CZM) approach.

(b) Effect of transverse constraint: Constrained long edge models were analysed to represent a finite width joint being extracted from a structural panel (Fig. 2b). The constrained boundary condition is derived from the fuselage global models using a global-local approach. Displacement field was

extracted from the global model of bonded fuselage barrel models and imposed on the local models as the boundary condition.

(c) Effect of joggle runout configuration: Detail design of a joggle runout configuration (Fig. 2c) in the global bonded fuselage barrel models are introduced for comparison with the standard SLJ. Debond damage propagation behaviour with the two local detail configurations is modelled.

(d) Effect of initial damage: The damage tolerant design requirement assumes that initial damage (e.g. debond) exists. This work considers both through-width initial damage (typical for narrow width lab joints) and thumb-nail damage configuration (more realistic for wider joints and accidental damage), which were introduced into narrow and wide co-curing SLJ models, respectively, (Fig. 2d). The strain energy release rate (SERR), which drives the crack growth, was calculated for the two different initial damage types using the virtual crack closure technique (VCCT) [22, 23].

The possibility of joint failure by delamination of the composite adherend is acknowledged as a possible failure mechanism where the adherend contains pre-existing delamination damage and/or where the adhesive is particularly effective. However the main focus of this paper is the design and analysis of the composite joint and therefore the adherend delamination is not considered in this work.

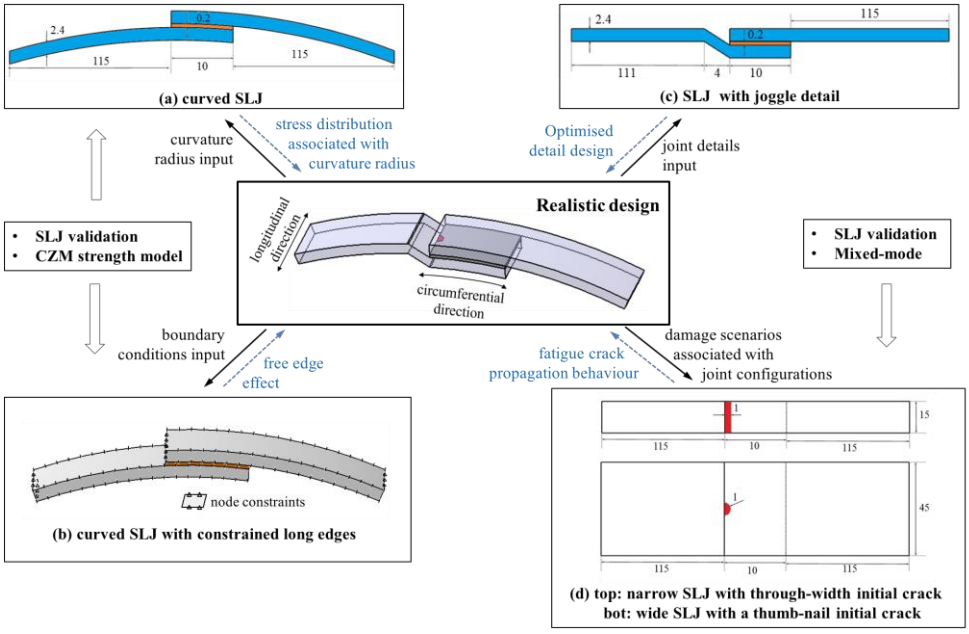

Fig. 2. Schematic of joint features and corresponding models: centre picture: design goal of a wide and curved lap joint with constrained long edges and initial damage; (a) curved narrow SLJ with free long edges, (b) narrow SLJ with joggle detail; (c) wide curved lap joint with constrained long edges extracted from global models, (d) narrow and wide lap joint with different initial damage scenarios (unit: mm)

Table 1 Summary of models used in the parametric study (schematic models in Fig. 2)

Refer to Fig. 2	Model code	SLJ (Standard runout)	SLJ (Joggle runout)	Flat	Curved	Long edges	Width (mm)	Initial Damage
Centre Picture	Design goal	X		X		free	15	No
(a)	SLJ-C-R3000	X			X	free	15	No
(b)	SLJ (Standard)-C-BC1	X			X	constrained	100	No
(b)	SLJ (Joggle)-C-BC1		X			constrained	100	No

(c)	SLJ (Joggle)		X	X		free	15	No
(d)	SLJ-Narrow	X (Co-curing)		X		free	15	Yes, through-width
(d)	SLJ-Wide			X		free	45	Yes, thumb-nail

Note: *W* represents the joint width. *R*3000 means curved lap joint with a radius of 3000 mm; for flat joint, $R=\infty$. BC1 represents the boundary condition 1 applied to the global model as illustrated in section 3.2 Fig. 5.

3. Model descriptions

3.1 SLJ: effect of curvature

The load-displacement response of the standard SLJ was modelled by Abaqus V6.14, using the same material properties and dimensions as the specimen tested in reference [21]. The specimen geometry is presented in Fig. 3a. Taking the typical fuselage diameters of narrow-body (3000-4000 mm) and wide-body aircraft (5000-6000 mm), respectively, this study considers curved SLJs with curvature radii of 1000, 2000, 3000 mm.

Adherends are made of 16 plies of unidirectional carbon-epoxy pre-preg of 0.15 mm ply thickness. The adhesive Aradite® 2015 is a two-component epoxy adhesive, which allows large plastic deformation prior to failure. The elastic properties of a unidirectional laminate and the adhesive are listed in Table 2. The adherends were modelled as elastic orthotropic with specified orientations in the FE model and the adhesive as isotropic. For the CZM, the adhesive was characterised with penalty stiffness in tension (K_{n}) and shear (K_{S}) (values were obtained through a calibration analysis), the failure strength in tension (t_{n}^{0}) and shear (t_{s}^{0}), and the fracture energy $G_{\mathrm{C}}^{\mathrm{n}}$ and $G_{\mathrm{C}}^{\mathrm{S}}$ are summarised in Table 3.

Table 2 Elastic properties of the adherend and the adhesive [21]

	E_x (GPa)	E_y (GPa)	E_z (GPa)	ν_{xy}	ν_{xz}	ν_{yz}	G_{xy} (GPa)	G_{xz} (GPa)	G_{yz} (GPa)
Adherend	109	8.819	8.819	0.342	0.342	0.380	4.315	4.315	3.2
Adhesive	1.85	1.85	-	0.330			-		

Table 3 Cohesive model parameters of the adhesive Araldite® 2015 for CZM modelling [21]

K_{n} (N/mm^3)	K_{s}(N/mm^3)	t_{n}^{0}(MPa)	t_{s}^{0}(MPa)	$G_{\mathrm{C}}^{\mathrm{n}}$ (N/mm)	$G_{\mathrm{C}}^{\mathrm{S}}$ (N/mm)
10000	10000	21.63	17.9	0.43	4.70

The finite element models for the flat and curved SLJ are depicted in Fig. 3. Four-node two-dimensional plane strain elements with incompatible modes (designated as CPE4I in Abaqus) were used for the laminates to avoid shear locking and four-node cohesive elements (COH2D4) for the adhesive. Solid element model in both the adherends and the adhesive were also conducted for comparison. To ensure numerical stability of cohesive elements, a mesh convergence study was conducted. The element sizes of 0.2×0.2 mm^2 at the bonded overlap area and 1×1 mm^2 at other areas were used to capture the stress variations accurately. Four elements in the laminate thickness direction [24] and a single row of cohesive element in the adhesive were modelled. Boundary conditions constrained the nodes at one edge in both longitudinal and transverse directions, while a perpendicular displacement was applied to the normal surface of the opposite edge.

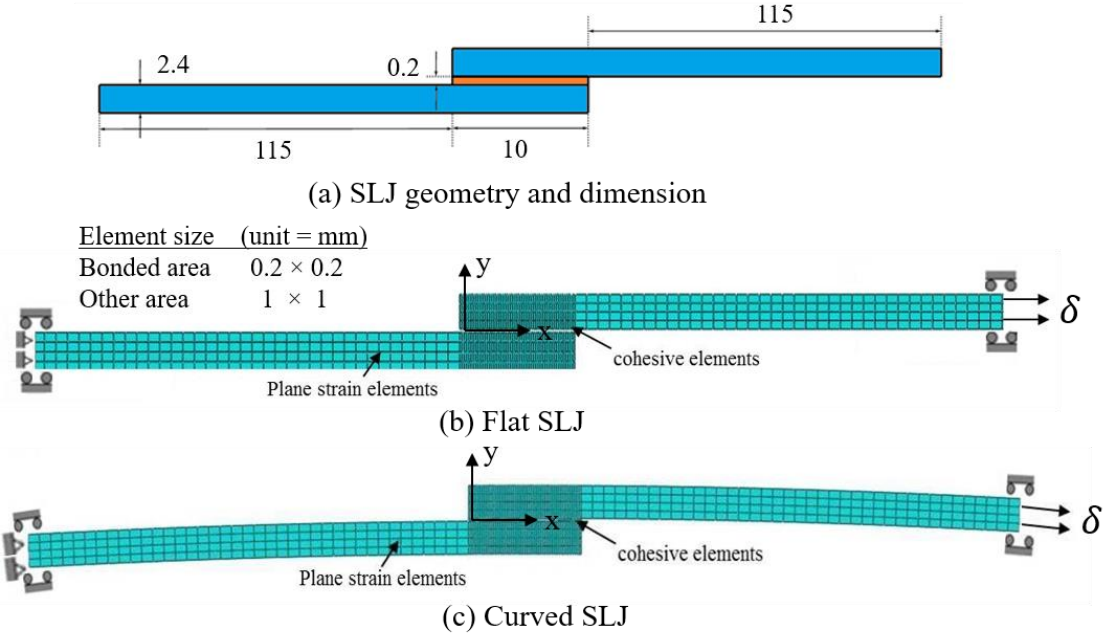

Fig. 3. (a) Geometry and dimension of standard SLJ [20], and finite element model and boundary conditions of (b) flat SLJ and (c) curved SLJ (adherends: plane strain elements, adhesive: cohesive elements; Element size: bonded area: 0.2×0.2 mm^2, other areas: 1×1 mm^2)

3.2 Joint geometry and constrained boundary conditions

A global-local modelling approach was adopted for the derivation of joint geometry and boundary conditions. Representative fuselage longitudinal joints (global model) and extracted curved SLJs (local models) are shown schematically in Fig. 4. The diameter of 2000 mm and the width of 500 mm were used for the global joint model. In this case, the geometry of the local curved SLJ was adopted to reflect the realistic fuselage design. In Fig. 4b, the curvature length of 4 mm for the joggle configuration is designed according to the geometry presented in reference [17]. In this category, the same material parameters of the adherends and the adhesive were used as the baseline model. Two composite layup sequences were studied for the adherends, which are $[0]_{16}$ (UD layup) and $[45_2/90_2/0_2/\text{-}45_2]_S$ (Quasi-Isotropic layup to simplify composite layup modelling).

In the global model, eight-node brick elements with incompatible modes (C3D8I) were used for the adherends and adhesive in the non-linear static FE analysis. A mesh convergence study gave a coarse mesh of 20 mm with an aspect ratio of 1 for the global model. As seen in Fig. 5b, the global model is analysed under three different boundary conditions (BC) under a pressure load of 0.06 MPa which represents the pressurisation difference of a civil airliner, and the contours represents the displacement magnitude to illustrate the effect of fuselage applied boundary conditions: BC1, assuming the bulkhead structure is connected rigidly to the fuselage barrel and infinitely stiff (no deformation), both ends are modelled by fixing the nodes in all directions and rotations; BC2, for simulation of the whole fuselage structure, the front and aft fuselage models were joined using the tie constraints, allowing for the longitudinal stress in the fuselage barrel and BC3, the fuselage barrel is assumed to be able to deform uniformly under inner pressure, MPC couplings were employed to restrain the displacements (including rotations) of the nodes at both ends to the referred fixed point.

The local models were run as a separate analysis with the link of time-dependent displacements and rotations on boundary nodes from the global analysis being transferred to the corresponded local SLJs. Strength analysis was conducted in Abaqus/Explicit analysis with the adhesive layer modelled as cohesive elements. A finer mesh was employed in the local model.

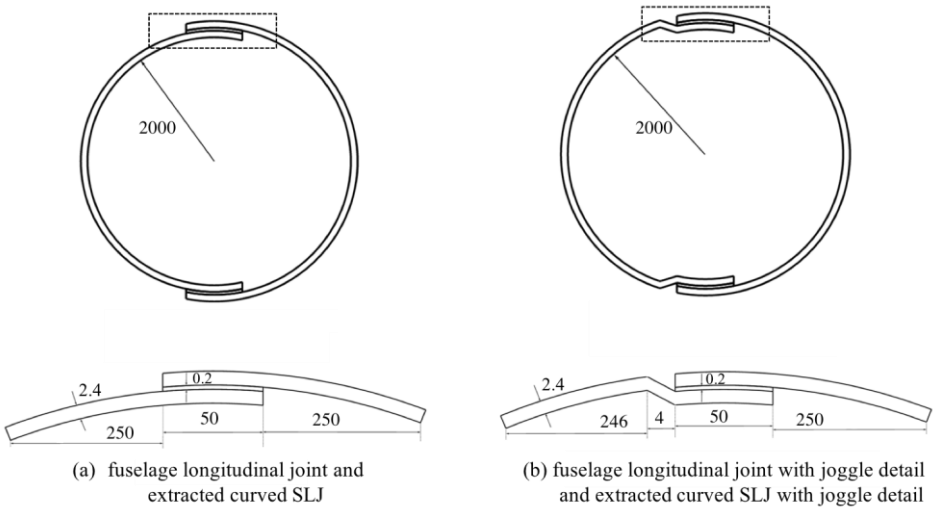

Fig. 4. Geometry of (a) fuselage longitudinal joint and extracted curved SLJ and (b) fuselage longitudinal joint with joggle detail and curved SLJ with joggle detail (unit: mm)

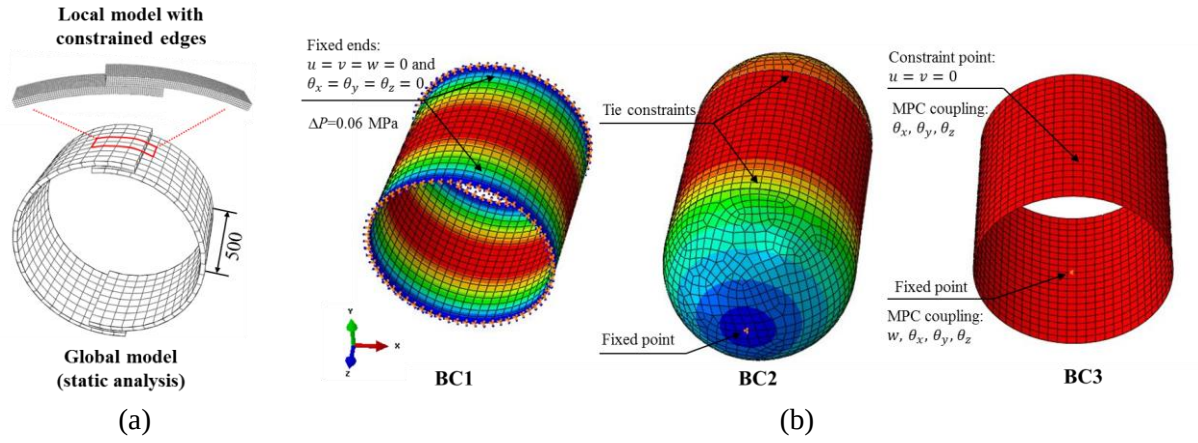

Fig. 5. (a) "Global-local" modelling approach by extracting a displacement field from the global model of bonded fuselage barrel models and interpolating boundary conditions for the local models (W=500 mm), (b) Global FE models with three different boundary conditions (BC1, BC2, and BC3) under a pressure difference of ΔP=0.06 MPa (representing passenger aircraft fuselage) and the colour contours represents the displacement magnitude under the applied boundary conditions (blue colour represents zero displacement and red colour represents maximum displacement)

3.3 Local details: Standard and Joggled joint run-outs

The local curvature inherent to the geometry of a joggle leads to uncertainties in the mechanical integrity of the SLJ. A detailed study has therefore been made of the stress distributions and SERR variations on the damage front within an SLJ with a joggle. A curvature length is introduced to the lower adherend to create the joggle configuration (knee) for comparison with the standard SLJ (refer

to Fig. 2c). Material parameters, modelling and loading conditions applied to the joggle configuration are the same as the baseline SLJ model.

3.4 Initial damage configurations

The standard SLJ is narrow (test specimens in the literature are usually around 20 mm wide) and the initial damage is artificially introduced as a uniform through-width edge crack (as per usual practice reported in the literature), as illustrated in Fig. 6a. This standard configuration is compared with wide single lap joints that have localised initial damage as shown in Fig. 6b or 6c. Both the standard and wide configurations were assumed to be manufactured by the co-curing procedure, with no adhesive between the top and bottom adherends. The length of the through-width crack in narrow SLJ and the radius of the thumb-nail crack in wide SLJ were presumed to be same, which is 1 mm in both cases. The adherends and adhesive used in this part of the study were the same as the baseline model of standard SLJ. The analysis was conducted on composite adherends with unidirectional layup.

Crack front strain energy release rate was calculated using the Virtual Crack Closure Technique (VCCT). The top and bottom adherends were connected by defining a set of bonded nodes. The crack propagation behaviour was carried out with a static load analysis by manually releasing the crack tip node along an assumed crack propagation pattern and modifying the bonded node set. In this study, two different crack propagation patterns were assumed: a concentric crack growth pattern (shown in Fig. 6b), and a transverse crack growth pattern (shown in Fig. 6c).

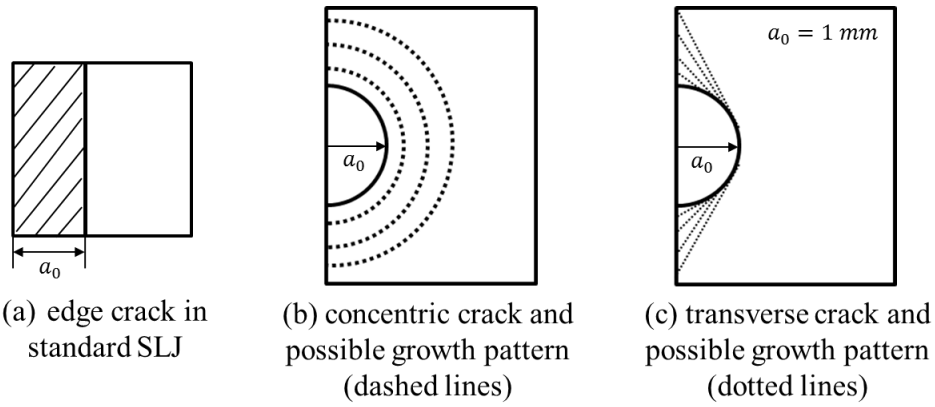

(a) edge crack in standard SLJ

(b) concentric crack and possible growth pattern (dashed lines)

(c) transverse crack and possible growth pattern (dotted lines)

Fig. 6: (a) Uniform edge crack in standard SLJ, (b) concentric crack growth from semicircular crack in wide SLJ, and (c) transverse crack growth from semicircular crack in wide SLJ

4. Results and discussion

4.1 Model verification and validation

Prior to the parametric study, verification of the baseline model was carried out by comparing the load-displacement response of SLJ simulated with both 2D plane strain elements and 3D solid elements with published FEA work [21], as shown in Fig. 7a. It can be seen that both 2D and 3D models predict the stiffness and the maximum load within 2%. The validation work was repeated with experimental results of an SLJ model with joggle detail configuration [17]. Good agreement was observed for the 2D models in Fig. 7b, although the 3D model over predicts the strength.

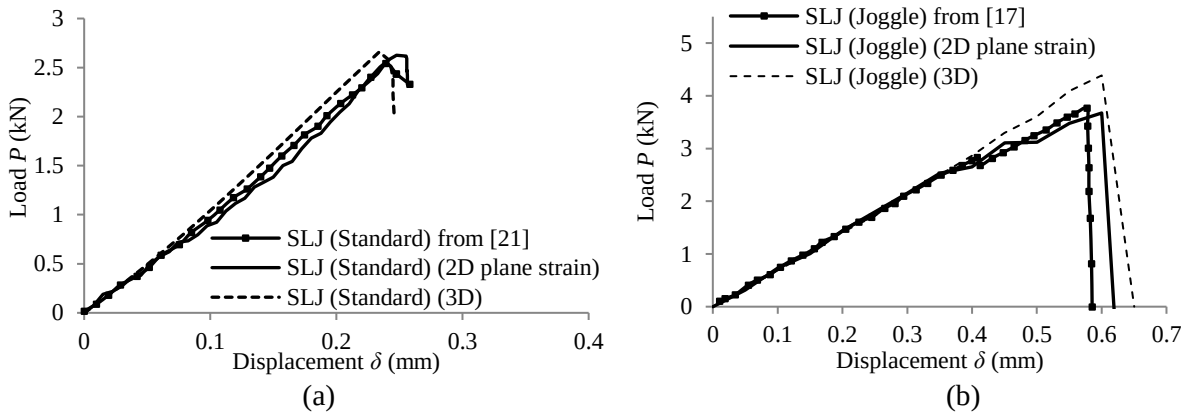

Fig. 7. Calculated *P-δ* curves and verification of (a) standard SLJ model with [21] and (b) SLJ with joggle detail comparison with [17]

4.2 SLJ: effect of joint curvature

In the parametric study of flat and curved SLJ, the adherends and the adhesive were modelled with 2D plane strain elements. The *P-δ* responses and peel stress along the overlap length of the adhesive in SLJ of various curvature radii are shown in Fig. 8. From Fig. 8a, it indicates that a moderate curvature has negligible effect on the peak load, although greater curvature results in larger displacements under uniaxial tension as the curved specimen straightens out. Additionally, curvature causes the peel stress at the runout of the adhesive bond reduce from tension to compression depending on the radius of the curve, as illustrated in Fig. 8b. For R ≥ 2000 mm with 2.4 mm specimen thickness, curvature has the same trends as flat joint. Therefore, flat joint specimens can be used in labs to simulate curved joints of R ≥ 2000 mm.

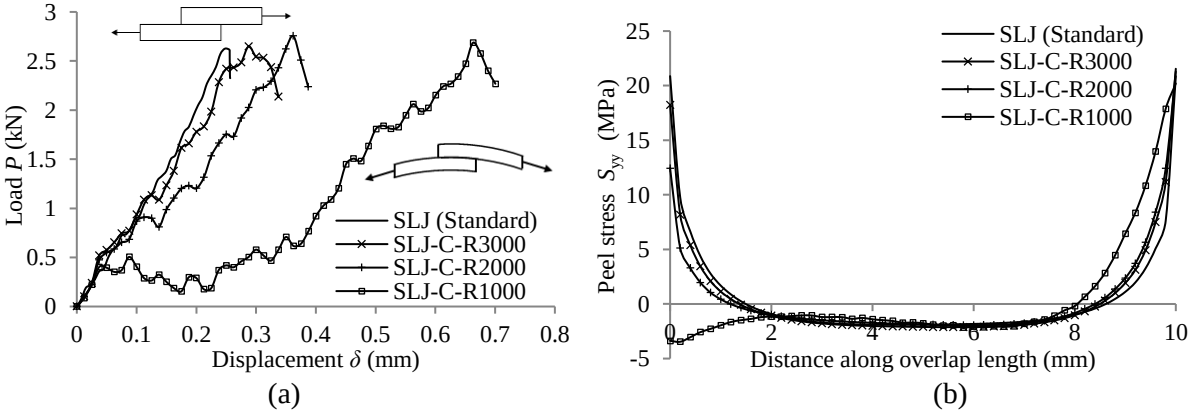

Fig. 8. (a) Load vs. displacement responses, (b) Peel stress distribution along the bond overlap length with various curvature radii (*P*=1 kN)

4.3 Effect of joint shape and boundary conditions

Predicted *P-δ* curves of curved SLJ with constrained edges are shown in Fig. 9 with comparison with standard SLJ. First, the predicted *P-δ* responses of the curved SLJ under three different boundary conditions are shown in Fig. 9a. It can be seen that, although there is a significant difference between constrained edges and free edges, the finer details of the constraint (i.e. BC1, BC2, or BC3) have

relatively little effect upon the load-displacement response. Therefore, when comparing flat vs curved and standard vs joggle SLJ configurations, only the free-edge and BC1 conditions are considered.

The predicted stiffness of flat SLJ (with free edges) with UD layup is about 3.8 times stiffer than curved joint (constraint edges); for QI composite layup, the ratio of stiffness is significantly reduced (about 2.6 times) owing to the reduced stiffness of QI laminate. Both of the curved SLJ (with standard or joggle runout) predict similar *P-δ* response as the bonded area is relatively small compared to the entire longitudinal fuselage structure. This research suggests that (a) the laboratory tests on flat specimens with free edges provide overly conservative results if applied directly to the design of component structures, (b) joggle detail does not affect *P-δ*, but will affect peel stress (Fig.10b).

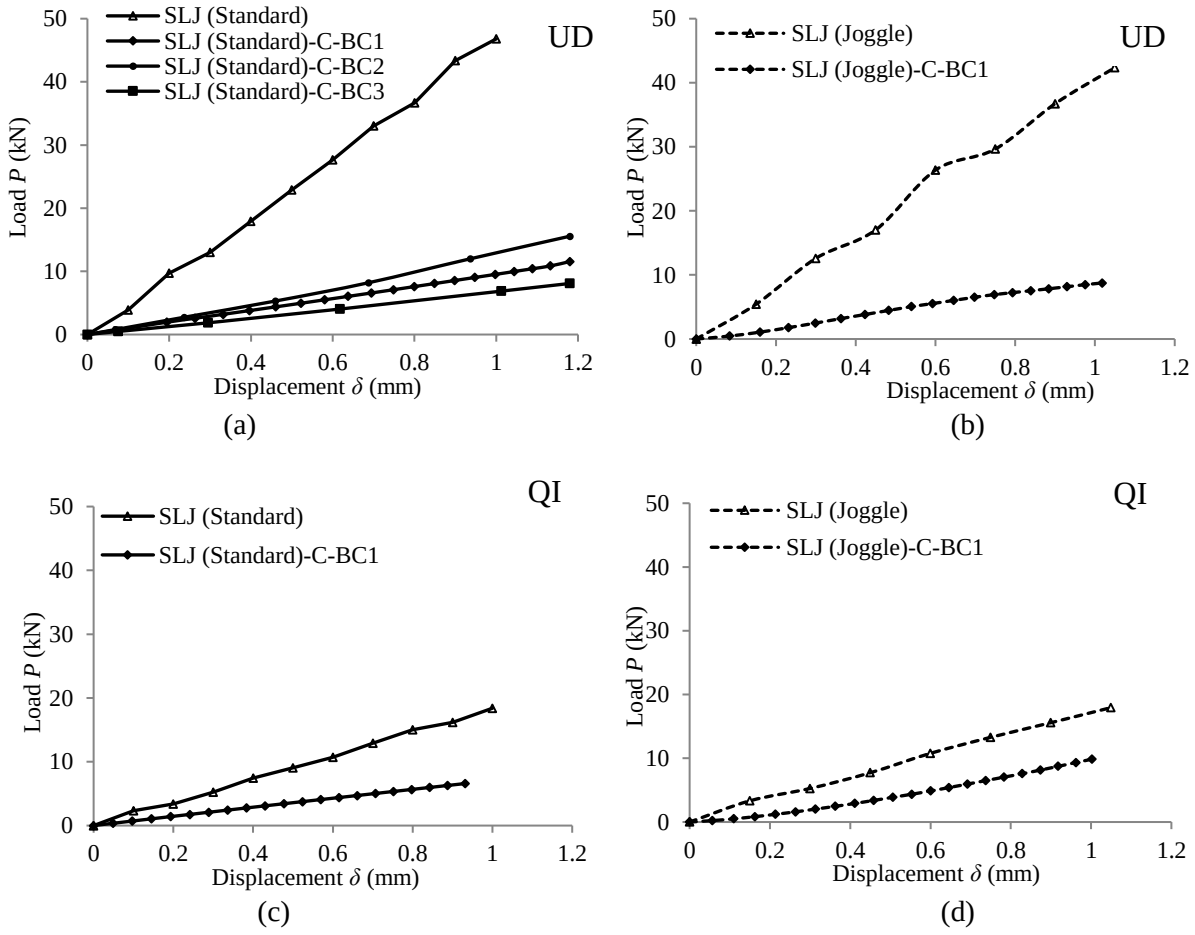

Fig. 9. Comparison of *P-δ* responses of SLJ (standard and joggle runouts) with free edge and curved joints with constrained edges: (a) SLJ (standard runout) with UD layup, (b) SLJ (joggle runout) with UD layup, (c) SLJ (standard runout) with QI layup, (d) SLJ (joggle runout) with QI layup

4.4 Local stresses in SLJs with standard or joggle runout

Models of SLJ with standard and joggle runout configurations were subjected to a tensile load of 1 kN. Figure 10 shows the peel stress and shear stress distributions along the overlap length of the lower surface in the adhesive. The local curvature of the joggle feature plays an important role in regulating the stress distribution. The peel and shear stresses in the joggled region are higher near the curved zone of the joggle joint due to the geometric discontinuity, and lower near the straight runout end of

the joint due to the stress relief behaviour. Due to the curvature in the adherend, the high peel and shear stresses will cause the joggle joint to experience a lateral deflection in the curved zone, which represents a possible damage initiation region. The deformation profiles of SLJ with standard and joggle configurations are compared in Fig. 11.

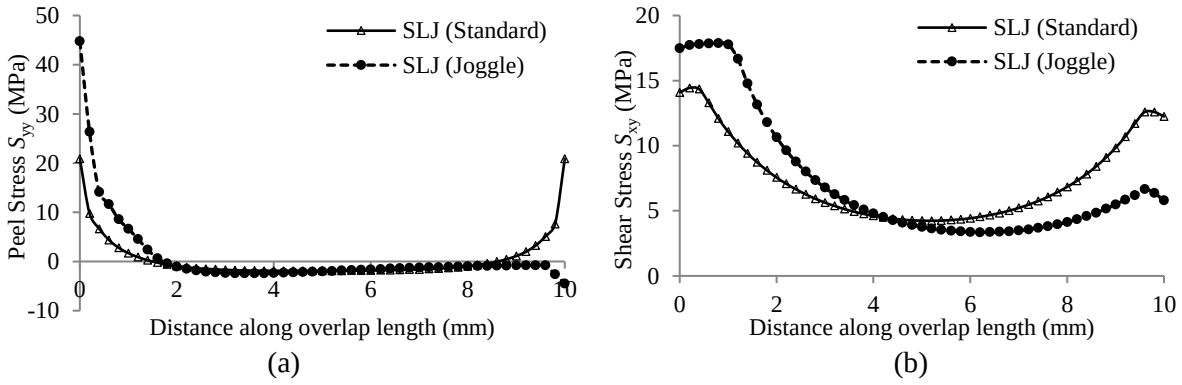

Fig. 10. Comparison of (a) peel stress and (b) shear stress along the lap length of the adhesive between SLJ (standard) and SLJ (joggle) (P=1 kN)

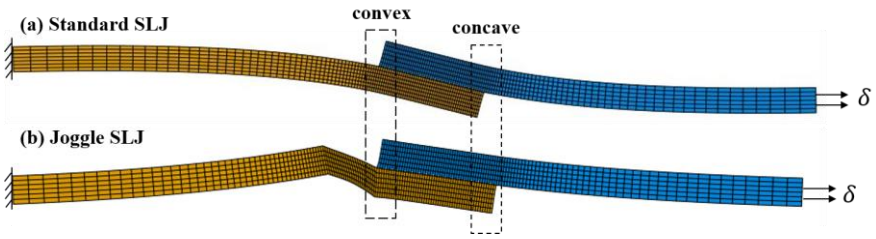

Fig. 11. FE calculated deformation plots of (a) standard SLJ and (b) joggle SLJ (scale factor=5)

In this part of the study, damage was assumed at the adherend-adhesive interface concerning the worst scenario in the damage tolerance design. Two possible crack initiation positions have been investigated: from the convex and concave runouts highlighted on Fig. 11. VCCT was used to calculate the Strain Energy Release Rate (SERR), which is the driving force to propagate crack, by performing FE analysis of different crack lengths for an applied displacement of 0.2 mm. Figure 12 shows the variation of SERR of different load modes (namely G_{I} and G_{II}, since the G_{III} values are insignificant for this geometry) with crack lengths from convex and concave runouts obtained for the standard and joggle SLJ configurations. G_{I} and G_{II} of the joggle configuration are higher than the standard configuration due to the higher stress values in the curved region (knee). The crack propagates in a mixed-mode for both standard and joggle configurations.

Crack propagations from the convex and concave runouts behave similarly for the standard configuration, but are significantly different at either end of the joggle configuration:

- For the standard configuration, mode I dominates when the crack initiates from the convex end and at relatively small crack lengths. However, as the crack propagates, mode II becomes dominant,

and the difference between mode I and mode II increases due to the effect of secondary bending on a standard SLJ.

- For the convex end of the joggle configuration, G_I and G_{II} values are high at relatively short crack lengths, which can be attributed to the initial opening of the blunt crack. As the crack propagates, both G_I and G_{II} values reach approximately constant value, indicating less significant bending effect. When the crack initiates from the concave runout, for the joggle configuration, G_I and G_{II} values are relatively small compared to the convex crack and G_{II} follows the similar trend as the standard configuration, indicating that the joggle configuration has better performance when the crack initiates from the concave end.

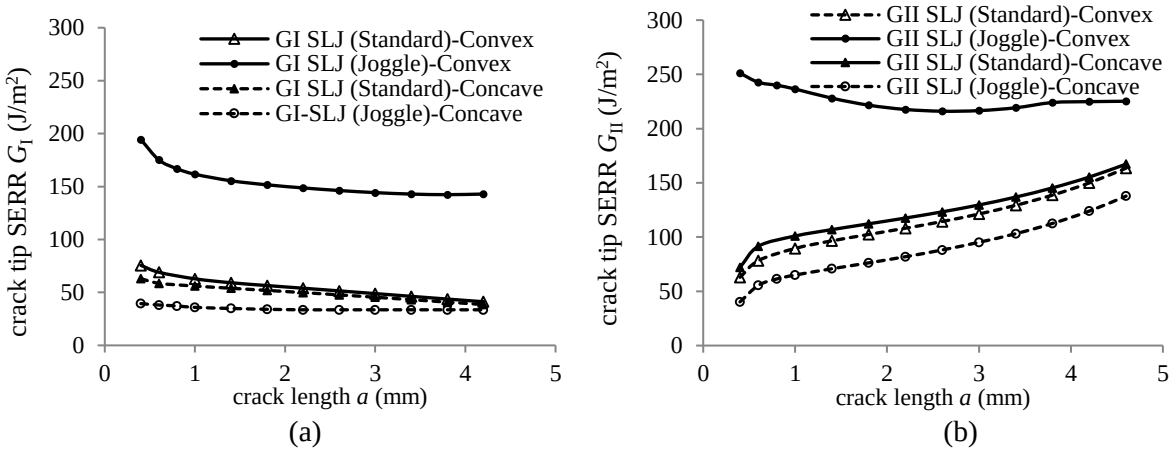

Fig. 12. SERR components of (a) G_I and (b) G_{II} vs. crack length a (from convex and concave runouts) in standard and joggle SLJ joints with adhesive failure (applied displacement of 0.2 mm)

4.5 SERR in narrow and wide SLJ with different initial damage configurations

Figure 13 illustrates the SERRs distribution along the damage front in the narrow and wide SLJ configurations. It is observed that the SERR is not constant along the damage front and there are sudden changes at the boundaries due to free edge effects. For the wide SLJ configuration, the SERRs along the circular damage front from -90º to 90º are shown in Fig. 13b. It can be seen that G_I is extremely high at ± 90º positions due to stress singularities, which indicates a high possibility of failure initiation and rapid propagation, and G_{II} is zero at ± 90º positions and reach the highest value at 0º position. At the 0º position in the thumb-nail crack, it can be seen that G_{II} is approximately 70 J/m^2, which is very similar to the G_{II} in the narrow specimen. This is as expected because the crack tip is perpendicular to the direction of loading in both cases.

Predicted G vs. a curves for two assumed crack propagation profiles are shown in Figure 14. Due to the symmetry condition (SERRs at ± 90º), the plots of SERRs at the -90º and 0 º positions are presented, which represent the two principal crack paths.

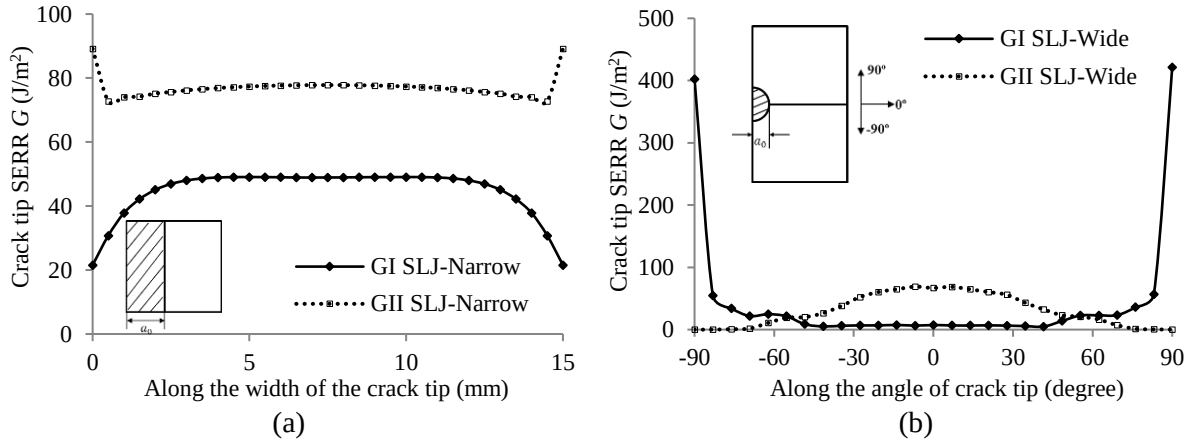

Fig. 13. Crack tip SERRs under applied displacement of 0.2 mm of (a) narrow SLJ with through-width crack, (b) wide SLJ with a thumb-nail crack

In the concentric crack growth pattern, at the -90º position, the mode I SERR is the highest, which predominately governs the crack propagation, whereas mode II is almost 0; at the 0º position, mode II is dominant. As the crack propagates, G_{II} increases and G_I decreases due to the bending moment experienced by the SLJ configuration.

For the transverse crack growth pattern, the most significant change is the mode II SERR at the -90º position. Figure 14b shows that mode I dominates at short crack lengths, but that as the crack propagates, mode II increases rapidly to play an important role in further crack propagation (which is due to the high shear stresses generated at the crack front of the assumed irregular crack profile). At the 0º position, the SERR reaches approximately a constant value soon due to the unchanged crack size at this point. This study on the variation of crack tip SERRs with crack length based on the above two assumptions thus provides a preliminary understanding on the crack propagation behaviour of the two SLJ configurations.

It can be summarised that an initial debond crack in wide SLJ configuration will propagate under a combination of the aforementioned two profiles and then, once the crack has reached the free edges, the same crack path as the narrow SLJ configuration will be followed.

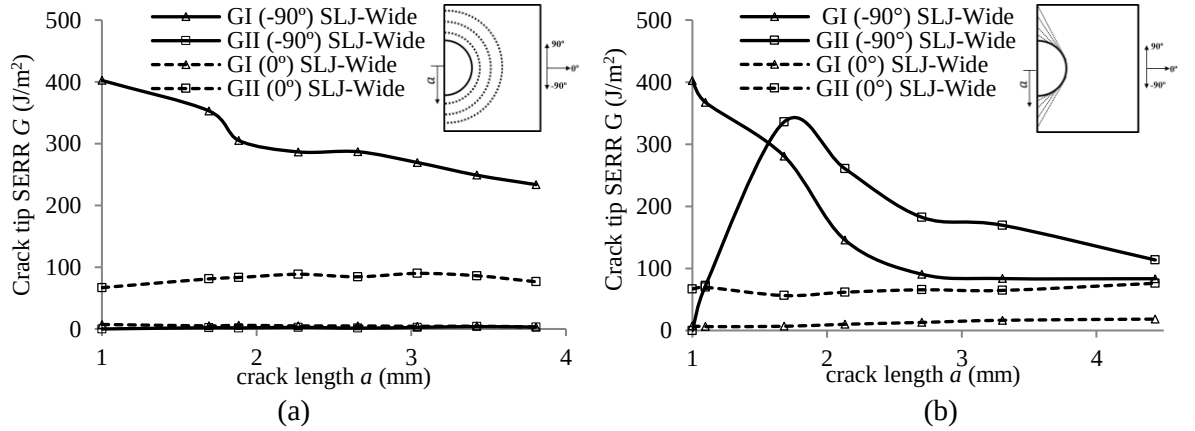

Fig. 14. SERRs vs. crack lengths in wide SLJ with two assumed crack growth patterns: (a) concentric crack growth pattern, (b) transverse crack growth pattern under an applied displacement of 0.2 mm

5. Conclusions

A parametric study was undertaken to investigate the effect of size, curvature and boundary conditions on the predicted strength of composite lap joints. Numerical analysis was applied, which incorporated non-linear geometric effects and cohesive zone models. Joint shape, width and boundary conditions were studied, together with two detail design features of joggled runout and initial damage location.

The main conclusions of these studies can be summarised as follows:

- Curvature has negligible effect on the lap joint peak load capacity if the radius is greater than 2000 mm (relevant to large transport aircraft fuselage).
- The free edge effect is a key issue for correctly predicting the strength of realistic joints by standard lab coupon joints; constrained long edges in wider joints have much higher strength. Therefore, the single lap joint geometry with free edges (such as used for conventional test coupons) provides conservative design to realistic joints with constrained edges.
- Compared to a standard joint runout, the proposed joggle design has lower peel stress and lower crack front strain energy release rate at the concave end of the bond runout. However, the joggle design results in higher peel stress and greater crack front strain energy release rate if crack initiates from the convex end. Despite the increased effective strength at the concave end of the joggle configuration, the convex end is effectively the weakest link in a curved SLJ and thus the decreased strength at the convex end means that the joggle configuration is ultimately more prone to debonding failure than the standard (non-joggle) configuration.
- According to the calculated strain energy release rates in modes I and II, a thumb-nail shape initial crack in a wide joint will initially propagate towards the two free edges to develop a through-width crack.

Acknowledgement

This research is funded by Coventry University, Faculty of Engineering, Environment and Computing, through a PhD studentship to Yiding Liu.

Reference

[1] Kinloch AJ. Toughening epoxy adhesives to meet today's challenges. MRS Buelletin 2003; 28: 445-448.

[2] Budhe S, Banea MD, de Barris S, da Silva LFM. An updated review of adhesively bonded joints in composite materials. Int J Adhes Adhes 2016; 72; 30-42.

[3] Harris L. The challenges in airbus to replace full scale aircraft fatigue testing by predictive virtual testing. 29th ICAF symposium 2017, Nagoya, June 2017.

[4] Volkersen O. Die nietkraftverteilung in zugbeanspruchten mit konstanten laschenquerschritten. Luftfahrtforschung 1938; 15: 41-47.

[5] Panigrahi SK, Pradhan B. Three dimensional failure analysis and damage propagation behavior of adhesively bonded single lap joints in laminated FRP composites. Journal of Reinforced Plastics and Composites 2007; 26 (2): 183-201.

[6] Sawa T, Liu JM, Nakano K, Tanaka J. A two-dimensional stress analysis of single-lap adhesive joints of dissimilar adherends subjected to tensile loads. J Adhes Sci Technol 2000; 14 (1): 43–66.

[7] Goncalves JPM, de Moura MFSF, de Castro PMST. A three-dimensional finite element model for stress analysis of adhesive joints. Int J Adhes Adhes 2002; 22 (5): 357–365.

[8] Campilho RDSG, de Moura MFSF, Domingues JJMS. Using a cohesive damage model to predict the tensile behaviour of CFRP single-strap repairs. Int J Solids Struct 2008; 45: 1497-1512.

[9] da Silva LFM, Campilho RDSG. Advances in numerical modelling of adhesive joints. Heidelberg: Springer; 2011.

[10] Campilho RDSG, Banea MD, Neto JABP, da silva LFM. Modelling adhesive joints with cohesive zone models: effect of the cohesive law shape of the adhesive layer. Int J Adhes Adhes 2013; 44: 48-56.

[11] Rocha RJB, Campilho RDSG. Evaluation of different modelling conditions in the cohesive zone analysis of single-lap bonded joints. J. Adhesion 2017; 1-21.

[12] Ascione F, Mancusi G. Curve adhesive joints. Compos Struct 2012; 94: 2657–64.

[13] Parida SK, Pradhan AK. Influence of curvature geometry of laminated FRP composite panels on delamination damage in adhesively bonded lap shear joints. Int J Adhes Adhes 2014; 54: 57-66.

[14] Muller RPG. An experimental and analytical investigation on the fatigue behaviour of fuselage riveted lap joints: The significance of the rivet squeeze force, and a comparison of 2024-T3 and Glare 3. PhD thesis, TU Delft, Delft, 1995.

[15] Skorupa A, Skorupa M. Riveted lap joints in aircraft fuselage: design, analysis and properties. Dordrecht, Heidelberg, New York, London: Springer; 2012.

[16] Vlieger H, Ottens HH. Results on uniaxial and biaxial tests on riveted fuselage lap joint specimens. Report NLR CR 97319 L. NLR, Amsterdam, 1997.

[17] Tail AA, Boukhili R, Achiou S, Boukhili H. Bonded joints with composite adherends. Part II. Finite element analysis of joggle lap joint. Int J Adhes Adhes 2006; 26: 226–236.

[18] Ribeiro AB, Borges L, d' Almeida JRM. Numerical stress analysis of carbon-fibre-reinforced epoxy composite single-lap joints. Int J Adhes Adhes 2011; 31 (5): 331-7.

[19] Ribeiro FMF, Campilho RDSG, Carbas RJC, da Silva LFM. Strength and damage growth in composite bonded joints with defects. Compo Part B 2016; 100: 91-100.

[20] Lewis SJ. The use of carbon fibre composites on military aircraft. Compos Manuf 1994; 5: 95-103.

[21] Campilho RDSG, Banea MD, Neto JABP, da Silva LFM. Modelling adhesive joints with cohesive zone models: effect of the cohesive law shape of the adhesive layer. Int J Adhes Adhes 2014; 44: 48-56.

[22] Rybicki EF, Schmueser DW, Fox J. An energy release rate approach for stable crack growth in the free-edge delamination problem. J Compos Mater 1977; 11: 470-487.

[23] Krueger R. Virtual crack closure technique: History, approach and applications. Appl Mech Rev. 2004; 57: 109-143.

[24] Diaz J, Romera L, Hernandez S, Baldomir A. Benchmarking of three-dimensional finite element models of CFRP single-lap bonded joints. Int J Adhes Adhes 2010; 30 (3): 178–189.